actuators

MDPI

Article

Comparative Analysis of Armature Structure on Constant Force Characteristics in Long-Stroke Moving-Iron Proportional Solenoid Actuator

Rongkai Shang [1,2], Peng Liu [3,*], Wenwen Quan [3] and Yuwen Ouyang [3]

[1] Liaoning Provincial Key Laboratory of Energy Storage and Utilization, Yingkou Institute of Technology, Yingkou 115014, China
[2] College of Mechanical and Power Engineering, Yingkou Institute of Technology, Yingkou 115014, China
[3] College of Automotive and Mechanical Engineering, Changsha University of Science & Technology, Changsha 410114, China
* Correspondence: liupeng@csust.edu.cn

Abstract: The influence of key design parameters on the constant force characteristics of long-stroke moving-iron proportional solenoid actuators (MPSAs) has been explored by a method combining finite element modelling and correlation analysis. First, the finite element model (FEM) of long-stroke MPSA was developed and validated. Subsequently, the two evaluation indexes, the average-output solenoid force and maximum-output solenoid force variability, were introduced to disclose the influence law of pole shoe parameters on the constant force characteristics of a long-stroke MPSA. After that, correlation analysis was employed to quantify the influence of several parameters and parameter interaction factors on the constant force characteristics. The results indicate a strong contradiction between the average-output solenoid force and maximum-output solenoid force variability; however, increasing the inner diameter of the cone helps enhance the average-output solenoid force without causing maximum-output solenoid force variability to increase. Among all the parameters examined, the cone angle is the most significant parameter affecting the constant force characteristics. Additionally, interactions between the cone angle and the cone length, the cone angle and the inner cone diameter, the cone angle and the outer cone diameter, the cone length and the outer cone diameter, as well as the inner cone diameter and the outer cone diameter also have an important influence on the constant force characteristics. This study deepens our understanding of how the key parameters affect the constant force characteristics and assists designers in optimizing these parameters for developing new structures.

Keywords: proportional solenoid actuator; constant force characteristics; average electromagnetic force; electromagnetic force fluctuation; correlation

check for updates

Citation: Shang, R.; Liu, P.; Quan, W.; Ouyang, Y. Comparative Analysis of Armature Structure on Constant Force Characteristics in Long-Stroke Moving-Iron Proportional Solenoid Actuator. *Actuators* **2024**, *13*, 408. https://doi.org/10.3390/act13100408

Academic Editors: Feng Sun, Zhiqiang Long, Suyuan Yu, Jin Zhou, Ran Zhou and Chuan Zhao

Received: 26 August 2024
Revised: 30 September 2024
Accepted: 5 October 2024
Published: 8 October 2024

Copyright: © 2024 by the authors. Licensee MDPI, Basel, Switzerland. This article is an open access article distributed under the terms and conditions of the Creative Commons Attribution (CC BY) license (https://creativecommons.org/licenses/by/4.0/).

1. Introduction

The moving-iron proportional solenoid actuator (MPSA) is widely used as an automatic control element in many fields due to its simple structure, large driving force, and low cost [1–3]. The applications include robotic control [4], common rail systems with direct injection in diesel engines [5], hydraulic braking actuators in automobile ABSs [6], automatic transmission pressure control devices [7], and hydraulic systems [8–10]. The relationship between the coil current of the MPSA and the output driving force is directly proportional. Thus, both the external driving force and the displacement of the controlled object can be regulated by adjusting the coil current signal. A good consistent force characteristic of the MPSA is crucial for accurately controlling the displacement of a controlled object. This implies that the output solenoid force of the MPSA is solely a linear function of the coil current and is independent from the stroke, representing a horizontal stroke force characteristic [11,12].

Presently, research indicates that the constant force characteristic of the MPSA is mainly determined by the shape of the pole shoe. Many scholars have examined the structural characteristics and mechanisms of influence associated with pole shoes. XU et al. [13] developed a precise model for the proportional solenoid valve, taking into account the magnetic saturation of soft magnetic materials as well as the flow force exerted by the valve spool. This model serves as a valuable tool for optimizing system design. WANG et al. [14] established models of a proportional solenoid actuator for magnetostatic finite element analysis in both two and three dimensions. They validated these models by comparing the static push force between the two-dimensional finite element model (FEM), three-dimensional FEM, and the experimental results. Additionally, they devised a genetic algorithm-based static multi-objective optimization strategy to improve the static push force of the actuator by optimizing its structural parameters. As a result of this optimization strategy, there was a 21.8% increase in the average static push force during operation stroke. YUN et al. [5] investigated the impact of the gap between the plunger and control cone, as well as the dimensions of control cone, on the constant force characteristic of the MPSA for diesel engine common rail systems. They also utilized the finite element method to optimize the shape of the control cone. ZHNG [15] conducted analysis on the impact of the current intensity, the armature length, the rear angle of the iron core, and the secondary air gap on the constant force characteristic. YUAN et al. [16] conducted a study on the pole shoe structure of a flat-type proportional solenoid actuator and conducted detailed analysis of the impact of six different magnetic materials and geometric parameters on the constant force characteristics. YUN et al. [17,18] examined the attraction force characteristics of an electromagnetic proportional solenoid actuator in a pressure control valve by varying the dither like the PWM signal and optimized the structural parameters of the control cone. YU et al. [19] developed and validated a proposed three-dimensional FEM of a proportional solenoid. They demonstrated that certain key shape parameters have significant effects on electromagnetic force through parameter sensitivity analysis and made adjustments to optimize the model.

On the other hand, numerous scholars have conducted extensive research on the design and optimization of pole shoe structures. MENG et al. [20] proposed a novel modulation method to enhance the constant force characteristic of proportional solenoid actuators by introducing a by-pass air gap. Furthermore, they optimized the structural parameters of the proportional solenoid actuator with a by-pass air gap using a multi-objective optimization algorithm based on particle swarm. DING et al. [21] developed a new oil-immersed proportional actuator that is pressure-resistant, featuring a magnetic grid magnetic-isolated ring instead of the traditional magnetic-isolated ring structures. This design simplifies the manufacturing process by reducing the need for welding compared to that of magnetic-isolated ring structures made of nonmagnetic material. WANG et al. [22,23] conducted the optimization of the structural parameters of a pole shoe and the moving core of an MPSA by employing a combination of two-dimensional FEM and a multi-objective genetic algorithm. LIU et al. [24] optimized the pole shoe shape and working air gap size in an MPSA through a multi-objective optimization method based on traditional surrogate models and machine learning techniques. This resulted in an improvement of the constant force characteristic of the MPSA.

Although there are many precedents on the effect of the magnetic material types, the driving current, and the pole shoe structure parameters on the constant force characteristics of the MPSA, the above studies provide a good basis for improving the constant force characteristics of the MPSA. They mainly center on research on MPSAs with small strokes (an effective working stroke is less than 2 mm), with only a few reports on research on long-stroke MPSAs. The long-stroke MPSA can be used as direct actuators for high-power diesel engine speed control systems [25], vehicle robot driving [3], and so on, as well as for potential applications in electrohydrodynamic pump systems [26].

In addition, the existing precedents mostly provide qualitative analysis and subjective judgments regarding the influence of various key factors on the constant force characteristics of MPSAs. However, the quantitative indexes for evaluating such influences are still lacking. Furthermore, previous research has primarily analyzed the constant force

characteristics from the perspective of the overall solenoid force, ignoring the influence of the combination of the axial solenoid force F_1 acting on the armature end face and the additional axial solenoid force F_2 acting on the armature taper.

Moreover, previous research mainly focuses on the respective effect of some single factors on the constant force characteristics and does not pay more attention to the effect of parameter interaction factors. Therefore, the quantitative analysis of the influence of key design parameters on the constant force characteristics for long-stroke MPSAs is insufficient for research, and an investigation of the interaction factors of these parameters on the constant force characteristics needs to be conducted.

This study focuses on a long-stroke MPSA with a working stroke of 20 mm and an effective working stroke of 10 mm as the research object. This study begins by describing the structure and working principle of the system, as well as identifying the key parameters for analysis. Subsequently, an electromagnetic FEM for the long-stroke MPSA is established and validated. Two evaluation indicators, namely the average-output solenoid force F_V and maximum-output solenoid force variability δ_{max}, are then introduced to assess the constant force characteristics of the long-stroke MPSA. Based on these indicators, combined with electromagnetic component force analysis, this study examines the influence laws of five key parameters on the constant force characteristics. Finally, using correlation analysis methods, this study quantifies both the degree of influence of these five parameters and their interactive effects on the constant force characteristics. It provides powerful theoretical guidance for further optimizing the design of long-stroke MPSAs. The primary contributions of this study are as follows:

(1) An introduction of two evaluation indexes, namely the average-output solenoid force and maximum-output solenoid force variability, to quantitatively evaluate the constant force characteristics of long-stroke MPSA.
(2) The revelation of the influence rules of the key design parameters on the constant force characteristics of long-stroke MPSAs from the perspective of the electromagnetic components.
(3) The quantification of the influence degree of parameters and their parameter interaction factors on the constant force characteristics of long-stroke MPSAs through correlation analysis.

2. Structure and Principle

Figure 1 is a structural sketch of a long-stroke MPSA, which mainly includes an actuator shell, a proportional solenoid shell, an armature, a coil skeleton, a coil, a reset spring, a reset spring collar, a transmission shaft, and an actuator cover. When the coil is electrified, the proportional solenoid shell, the armature, and the coil skeleton are magnetized.

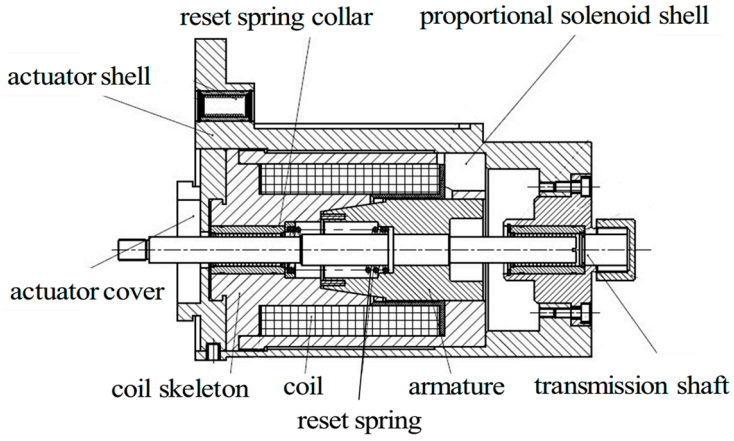


Figure 1. Structural sketch of long-stroke MPSA.

As shown in Figure 2, the main magnetic flux Φ is classified into two paths of magnetic fluxes Φ_1 and Φ_2. The magnetic flux Φ_1 is divided into two paths of magnetic fluxes Φ_{11} and Φ_{12}. The magnetic flux Φ_{11} enters the coil skeleton through the working air gap between the armature end face and the cone of the coil skeleton, while the magnetic flux Φ_{12} enters the coil skeleton through the working air gap between the armature end face and the bottom of the coil skeleton. The magnetic flux Φ_2 enters the coil skeleton through the working air gap between the armature taper and the coil skeleton taper.

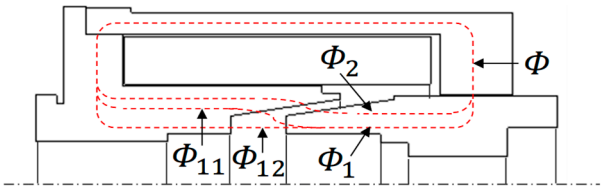


Figure 2. Magnetic circuit sketch of long-stroke MPSA.

With the approach of the armature to the coil skeleton, there is a gradual decrease in the reluctance of the working air gap between the armature tapers and the coil skeleton tapers in the magnetic flux Φ_2 loop. The degree of reduction is greater than that between the armature end face and the coil skeleton in the magnetic flux Φ_1 loop. This makes the magnetic flux Φ_1 gradually decrease, while the magnetic flux Φ_2 gradually increases, resulting in a decrease in the axial solenoid force F_1 acting on the armature end face and an increase in the additional axial solenoid force F_2 acting on the armature taper.

However, as the armature moves closer to the coil skeleton, there is a significant decrease in reluctance of the working air gap between the armature end face and the bottom of the coil skeleton, causing an increase in magnetic flux Φ_1. Thus, the axial solenoid force F_1 starts to increase.

As a result, the output solenoid force F obtained using a superposition of the two remains unchanged within a certain working stroke, i.e., it forms a horizontal stroke force characteristic, which is a constant force characteristic (as shown in Figure 3).

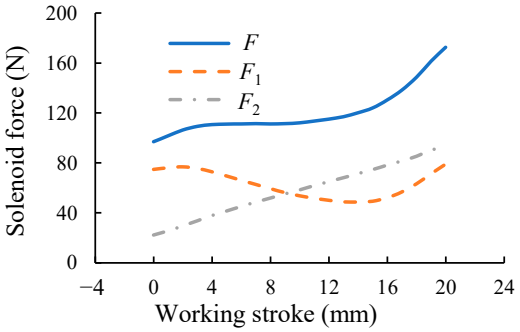


Figure 3. Stroke force characteristics of long-stroke MPSA.

3. Methodology

According to magnetic circuit analysis, the performance of an MPSA is mainly affected by the shape of the pole shoe and the size of the working air gap. Therefore, the key design parameters mainly include the pole shoe parameters and the air gap control parameters (armature initial position). The positions of specific parameters and their value ranges are shown in Figure 4 and Table 1. When studying the influence of one parameter, other parameters should be taken as reference values. However, when studying the influence of the cone inner diameter, the armature end width should be kept constant (the difference between the cone outer diameter and the cone inner diameter), as well as the other parameters at the reference values.

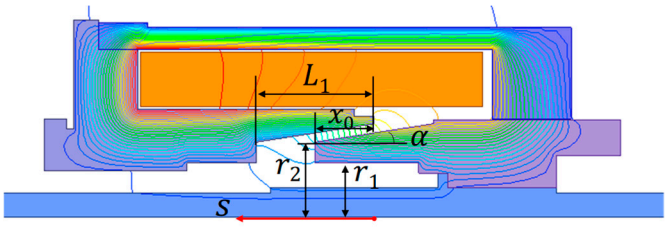


Figure 4. Schematic diagram of key parameters.

Table 1. The key design parameters and their value ranges.

Parameters	Ranges	Reference Value
Cone angle α (deg)	3–15	9
Cone length L_1 (mm)	20–32	24
Cone inner diameter r_1 (mm)	10–16	11
Cone outer diameter r_2 (mm)	12.25–18.25	15.25
The initial position of the armature x_0 (mm)	−4–8	2

To reveal the influence law of key parameters on the electromagnetic force of the long-stroke MPSA, the average-output solenoid force F_V (defined by Equation (1)) and maximum-output solenoid force variability δ_{max} (defined by Equation (2)) are employed to quantify this influence. These two indexes are used to quantitatively describe the overall standard of the electromagnetic force and the position of the maximum electromagnetic force, respectively. The output solenoid force F_S is equal to the resultant force of the axial solenoid force F_1 acting on the armature end face and the axial solenoid force F_2 acting on the armature taper, as shown in Equation (3). The axial solenoid forces F_1 and F_2 are calculated according to Equation (4). Through analysis of the electromagnetic component forces, a more comprehensive understanding of the influence mechanisms associated with the key parameters can be achieved.

$$F_V = \frac{\sum F_S}{n} \ (5 \le S \le 15, \ S \in \mathbf{N}) \tag{1}$$

$$\delta_{\max} = \max\{\delta_S\} = \max\left\{\left|\frac{F_S - F_V}{F_V}\right|\right\} \times 100\% \ (5 \le S \le 15, \ S \in \mathbf{N}) \tag{2}$$

$$F_S = F_1 + F_2 \tag{3}$$

$$F_i = \int_0^{2\pi}\int_0^{l} \rho_F \mathrm{d}l d\theta \quad (i = 1, 2) \tag{4}$$

where S represents the working stroke size; F_S represents the output solenoid force when the working stroke is S; n represents the calculated number of working strokes; δ_S represents output solenoid force variability when the working stroke is S, $\mathbf{N}$ represents a set of non-negative integers; ρ_F represents the edge force density, which can be derived from finite element analysis; and l represents the length of the end or cone of the armature.

Moreover, to further analyze the influence degree of each characteristic parameter and the interaction between characteristic parameters on the constant force characteristics of the long-stroke MPSA quantitatively, correlation analysis was conducted, and the correlation coefficient was used as the measurement index. The correlation coefficient is defined as follows:

$$R = \frac{\mathrm{cov}(X, Y)}{\sigma_X \sigma_Y}$$

where R is the correlation coefficient; $\mathrm{cov}(X, Y)$ is the covariance of variable X and variable Y; and σ_X and σ_Y are the standard deviation of variable X and variable Y, respectively.

The value range of the correlation coefficient is from −1 to +1, and the correlation strength is shown in Table 2. The larger the absolute value of the correlation coefficient is

and the higher the correlation strength is, the more significant the influence of one variable on another variable is, as the positive and negative signs of the correlation coefficient indicate the direction of influence [27]. Two hundred sample points and their response values were obtained by a uniform Latin Hypercube method based on the minimum correlation criterion [28] and the FEM of the long-stroke MPSA, and then correlation analysis was conducted in MODDE in this study.

Table 2. Information on correlation strength.

Correlation Strength	Absolute Value of Correlation Coefficient
Low	0~0.3
Medium	0.3~0.6
High	0.6~1

4. Finite Element Model and Its Verification

For this study, a two-dimensional FEM of a long-stroke MPSA was developed in ANSYS Maxwell. Due to the relatively closed magnetic circuit of the long-stroke MPSA, the magnetic lines of force are primarily concentrated in the magnetic circuit composed of soft magnetic materials, such as a proportional solenoid shell, an armature, a coil skeleton, and a transmission shaft; consequently, the magnetic flux leakage is minimal. Therefore, these components were predominantly considered in modeling. The boundary conditions are defined as balloon boundary conditions. The mesh element type utilized is triangular. The mesh was refined using an adaptive meshing method, with a 30% densification applied at each iteration until both the energy error and iteration error of the solution were reduced to less than 0.1%. The developed FEM is illustrated in Figure 5.

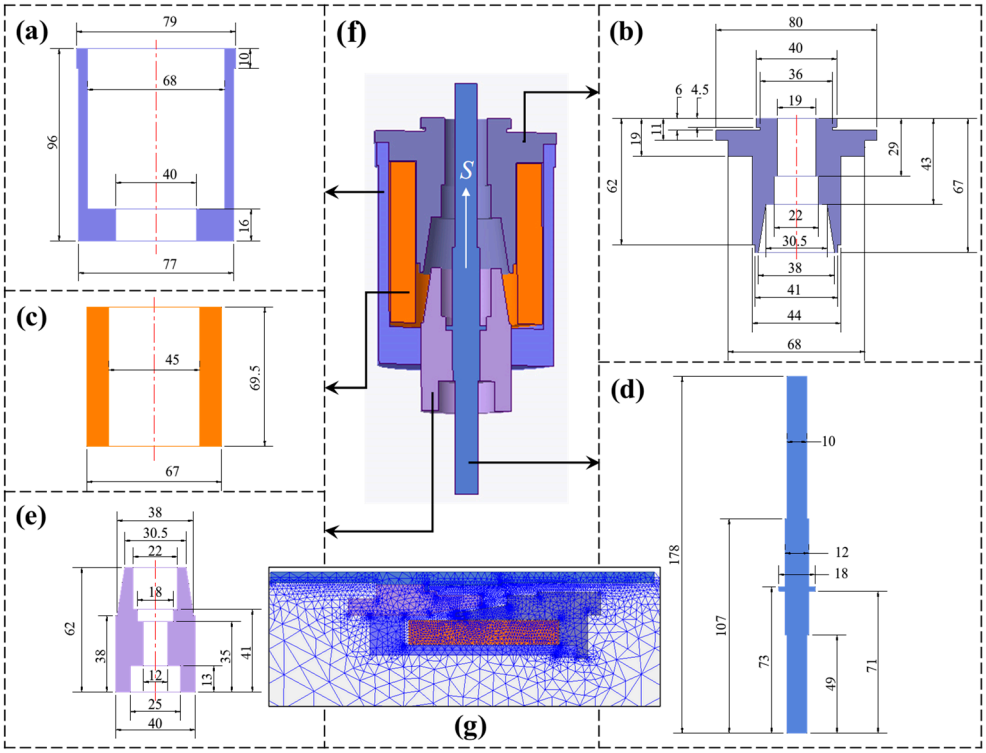


Figure 5. A simplified model of the actuator being studied: (**a**) a proportional solenoid shell; (**b**) a coil skeleton; (**c**) a coil; (**d**) a transmission shaft; (**e**) an armature; (**f**) an assembly model; (**g**) and a mesh demonstration.

Additionally, we have established an electromagnetic force test bench for the MPSA, as depicted in Figure 6. As shown in Figure 7, with the increase in drive current, the

output solenoid force correspondingly rises. The maximum relative absolute error of the solenoid force under all the working conditions is 4.3%, while the average relative absolute error is 2.3%. This discrepancy arises because the simulation model does not account for the hysteresis phenomenon present in soft magnetic materials; instead, a monotonic magnetization curve was employed to replace the actual magnetization curve. This substitution results in an inherent deviation between both the curves, and subsequently leads to calculational inaccuracies. Furthermore, during experimentation, a certain degree of static friction exists between the transmission shaft and bearing, which also contributes additional errors to the measurement of electromagnetic force. Overall, the simulation results presented in Figure 7 demonstrate good agreement with the experimental results. Further details regarding the model and its validation can be found in [29].

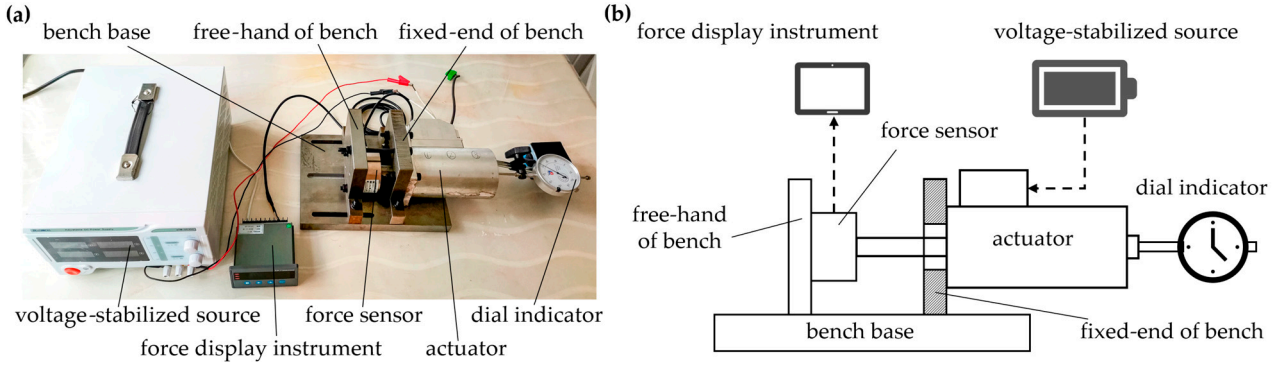


Figure 6. The electromagnetic force test bench for the MPSA: (**a**) a device photograph; (**b**) a schematic diagram.

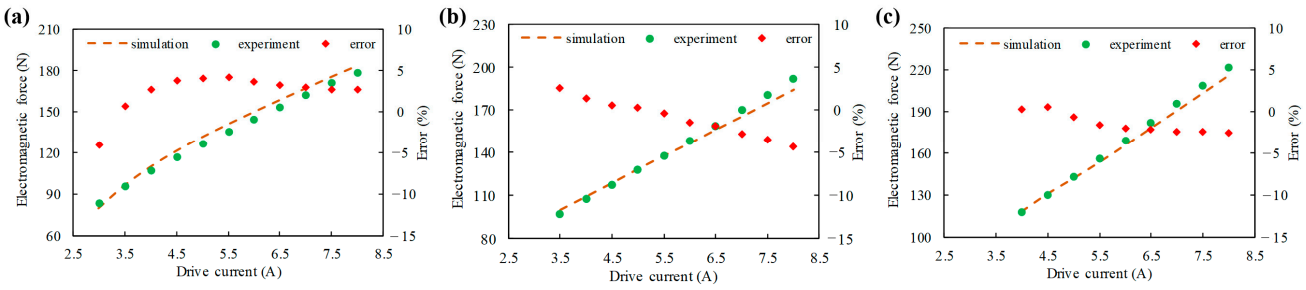


Figure 7. The result comparison of the simulation and the experiment: (**a**–**c**) with working strokes of 5 mm, 10 mm, and 15 mm, respectively.

5. Results and Discussion

5.1. Influence of Key Parameters

The changing situations of the average-output solenoid force F_V, output solenoid force variability δ_S and maximum-output solenoid force variability δ_{max} under the effect of these five key parameters were obtained by FEM. We observe that the average-output solenoid force F_V, output solenoid force variability δ_S and maximum-output solenoid force variability δ_{max} show different trends with different key parameter changes.

5.1.1. Cone Angle

It can be observed from Figure 8a,b that with the increase in the cone angle α, the average-output solenoid force F_V exhibits an approximately linear increase. Meanwhile, maximum-output solenoid force variability δ_{max} first decreases, and then increases, and maximum-output solenoid force variability appears at both ends of the effective working stroke. This phenomenon can be attributed to the occurrence of local magnetic saturation within the cone of the proportional electromagnetic actuator when the cone angle is small. However, as the cone angle increases, there is a corresponding increase in the cross-sectional

area of magnetic flux within the cone (as shown in Figure 8c), leading to alleviation of local magnetic saturation and consequently an increase in the output solenoid force due to the higher effective working magnetic flux.

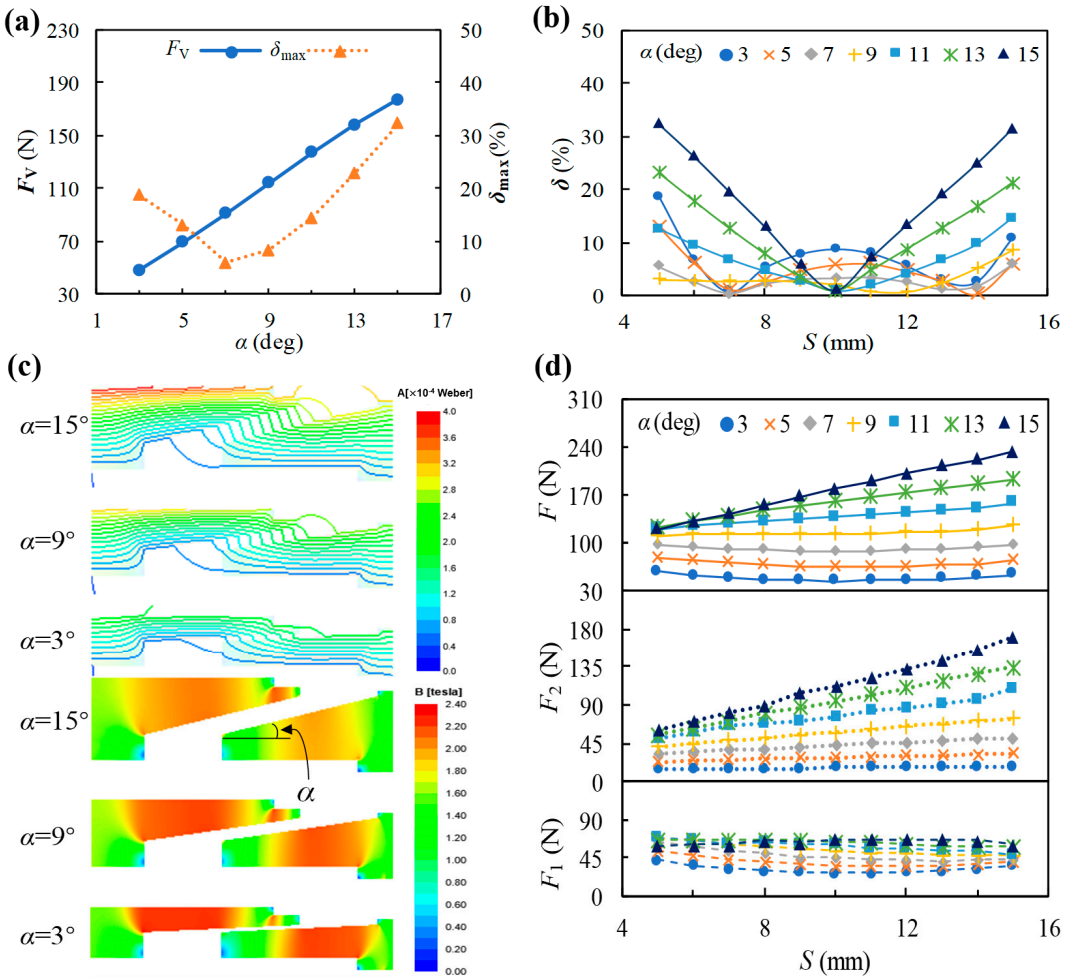


Figure 8. The influence of the cone angle on the constant force characteristics: (**a**) the average-output solenoid force and maximum-output solenoid force variability; (**b**) output solenoid force variability; (**c**) the magnetic field cloud map; (**d**) and the electromagnetic component forces.

Additionally, the change in the cone angle directly increases the suction area of the cone side and axial force acting on the cone side. This results in a greater influence of the cone angle on the additional axial solenoid force F_2 compared to the axial solenoid force F_1 (as shown in Figure 8d).

Meanwhile, the additional axial solenoid force F_2 increases approximately linearly with the stroke, and the growth rate continuously increases with the cone angle. For small cone angles, the axial solenoid force F_1 initially decreases, and then increases with the stroke, with a greater decrease in the axial solenoid force F_1 compared to the increase in the additional axial solenoid force F_2 at this point. As the cone angle reaches a certain value, the axial solenoid force F_1 decreases approximately linearly with increasing stroke. However, beyond a certain cone angle, the axial solenoid force F_1 will fluctuate as the stroke increases.

Therefore, an appropriate cone angle can be obtained to optimize the horizontal characteristics of the stroke force curve, thereby minimizing fluctuations in the output solenoid force.

5.1.2. Cone Length

From Figure 9a,b, it can be observed that as the cone length L_1 increases, the average-output solenoid force F_V approximately decreases linearly, while maximum-output solenoid force variability δ_{max} begins to decrease rapidly, and then gradually decreases. Additionally, it is noted that maximum-output solenoid force variability occurs at both ends of the effective working stroke. This phenomenon can be attributed to the fact that a longer cone results in a larger working air gap on the side of the cone, leading to increased magnetic resistance in the working magnetic circuit. Consequently, this reduces the effective working magnetic flux and lowers the magnetic induction intensity of the cone (as shown in Figure 9c), resulting in a lower output solenoid force.

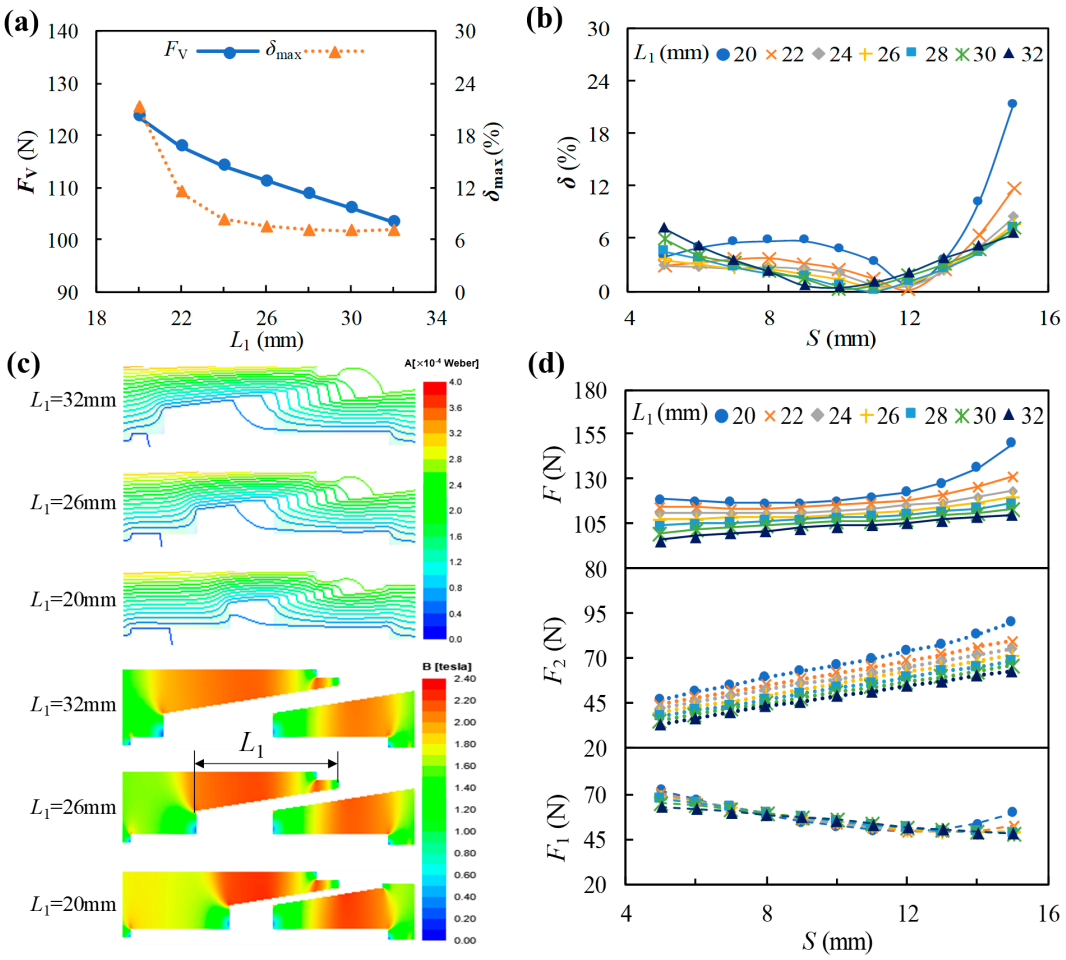


Figure 9. The influence of the cone length on the constant force characteristics: (**a**) the average-output solenoid force and maximum-output solenoid force variability; (**b**) output solenoid force variability; (**c**) the magnetic field cloud map; (**d**) and the electromagnetic component forces.

Furthermore, due to the larger excitation area for generating additional axial solenoid force F_2 compared to that for generating axial solenoid force F_1, the impact of changes in the working air gap caused by variations in the cone length on additional axial solenoid force F_2 is greater than that on the axial solenoid force F_1 (as shown in Figure 9d).

Simultaneously, the additional axial solenoid force F_2 approximately increases linearly with the increase in stroke, while the growth rate decreases gradually with the increase in cone length. When the cone length is small, the axial solenoid force F_1 first decreases, and then gradually increases with the increase in the stroke, and the decreasing degree of the axial solenoid force F_1 is less than the increasing degree of the additional axial solenoid

force F_2. When the cone length increases to a certain value, the axial solenoid force F_1 approximately decreases linearly with the increase in the stroke.

Consequently, with the increase in cone length, the growth rate of the additional axial solenoid force F_2, will be close to the decline rate of the axial solenoid force F_1, so that the stroke force curve will gradually level and the fluctuation rate of the output solenoid force will gradually decrease.

5.1.3. Cone Inner Diameter

As illustrated in Figure 10a,b, with the increase in cone inner diameter r_1, the average-output solenoid force F_V increases approximately linearly. Meanwhile, maximum-output solenoid force variability δ_{max} begins to increase rapidly, and then its growth rate decreases. Maximum-output solenoid force variability appears at the end of the effective working stroke. This occurs when the inner diameter of the cone becomes larger; the lateral cross-sectional area of magnetic flux in the cone of the proportional solenoid actuator increases, while the magnetic induction intensity of the cone remains unchanged (as shown in Figure 10c), thus increasing the output solenoid force.

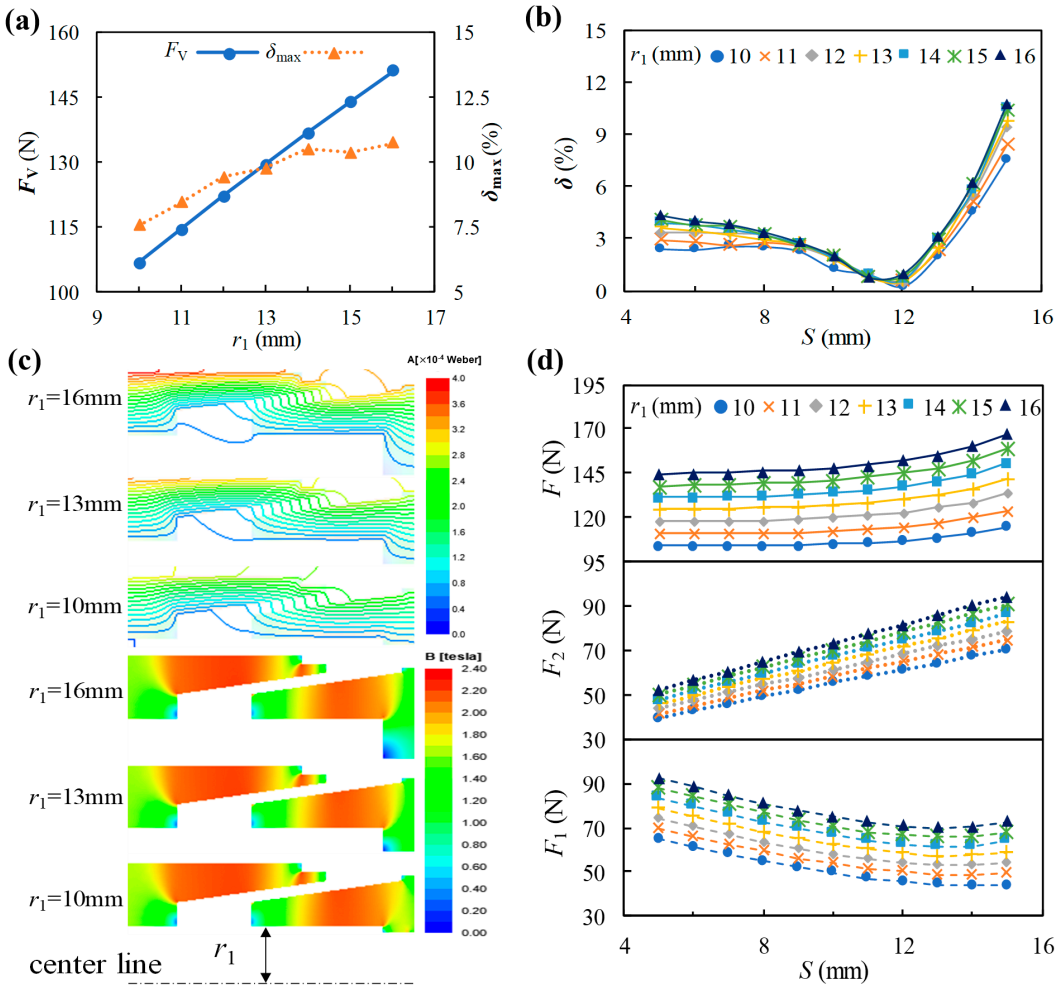


Figure 10. The influence of cone inner diameter on the constant force characteristics: (**a**) the average-output solenoid force and maximum-output solenoid force variability; (**b**) output solenoid force variability; (**c**) the magnetic field cloud map; (**d**) and the electromagnetic component forces.

Additionally, Figure 10d indicates that the additional axial solenoid force F_2 approximately increases linearly with the increase in the stroke, and the growth rate gradually increases with the increase in the inner diameter of the cone. In contrast, with the increase in stroke, the axial solenoid force F_1 approximately decreases linearly at first, and then grad-

ually decreases, while the decreasing degree of the axial solenoid force F_1 is not affected by the change in cone inner diameter. However, at the initial cone inner diameter, the decrease rate of the axial solenoid force F_1 is the closest to the increase rate of the additional axial solenoid force F_2, with the stroke force curve tending to be the most horizontal at this time. As the inner cone diameter increases, there is also a gradual increase in maximum-output solenoid force variability.

5.1.4. Cone Outer Diameter

According to Figure 11a,b, with an increase in the outer cone diameter r_2, the average-output solenoid force F_V approximately increases linearly. Meanwhile, maximum-output solenoid force variability δ_{max} first decreases, and then gradually increases, and maximum-output solenoid force variability appears at the end of the effective working stroke. The reason for this performance lies in the fact that when the outer diameter of the cone is small, there is a serious local magnetic saturation phenomenon in the cone of the armature of the proportional solenoid actuator. However, as shown in Figure 11c, with an increase in the outer diameter, there is an alleviation of this local magnetic saturation due to an increase in the cross-sectional area of magnetic flux within the cone of the armature. As a result, there is an increment in the effective working magnetic flux, leading to an increase in the output solenoid force.

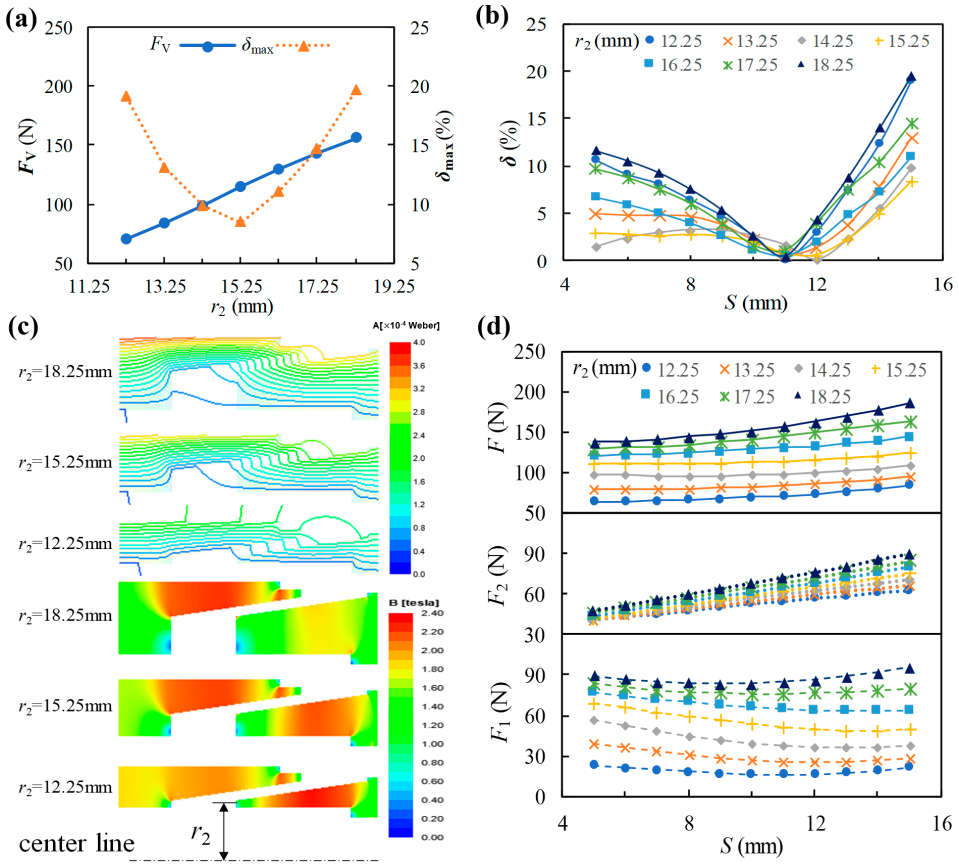


Figure 11. The influence of cone outer diameter on the constant force characteristics: (**a**) the average-output solenoid force and maximum-output solenoid force variability; (**b**) output solenoid force variability; (**c**) the magnetic field cloud map; (**d**) and the electromagnetic component forces.

Moreover, Figure 11d shows that the additional axial solenoid force F_2 approximately increases linearly with the increase in the stroke, and the growth rate gradually increases with the increase in the outer diameter of the cone. However, when the outer diameter of the cone is small, the axial solenoid force F_1 remains unchanged with the increase in the cone's outer diameter within a specific range. The increase in the axial solenoid force

F_1 at the initial end of the effective working stroke is larger than that at the end of the effective working stroke, resulting in a gradual decrease in the axial solenoid force F_1 with an increasing working stroke and a faster decrease rate with larger cone outer diameters. While the cone outer diameter increases beyond a specific value, the decrease rate of the axial solenoid force F_1 gradually decreases.

Thus, with the increase in outer cone diameter, the increase in additional axial solenoid force F_2 first approaches the decrease rate of axial solenoid force F_1, and then will be greater than its decrease rate. Hence, maximum-output solenoid force variability decreases first, and then gradually increases.

5.1.5. Initial Position of the Armature

As shown in Figure 12a,b, with the increase in the initial position of the armature x_0, the average-output solenoid force gradually increases, while maximum-output solenoid force variability δ_{max} first decreases, and then increases significantly, with maximum-output solenoid force variability appearing at the end of the effective working stroke. It is noticeable that a larger initial diameter of the armature results in a smaller working air gap between the armature and the coil skeleton, leading to less magnetic resistance, a larger working magnetic flux, and a stronger magnetic field (as shown in Figure 12c). Therefore, a larger average-output solenoid force is observed when there is a larger initial diameter of the armature.

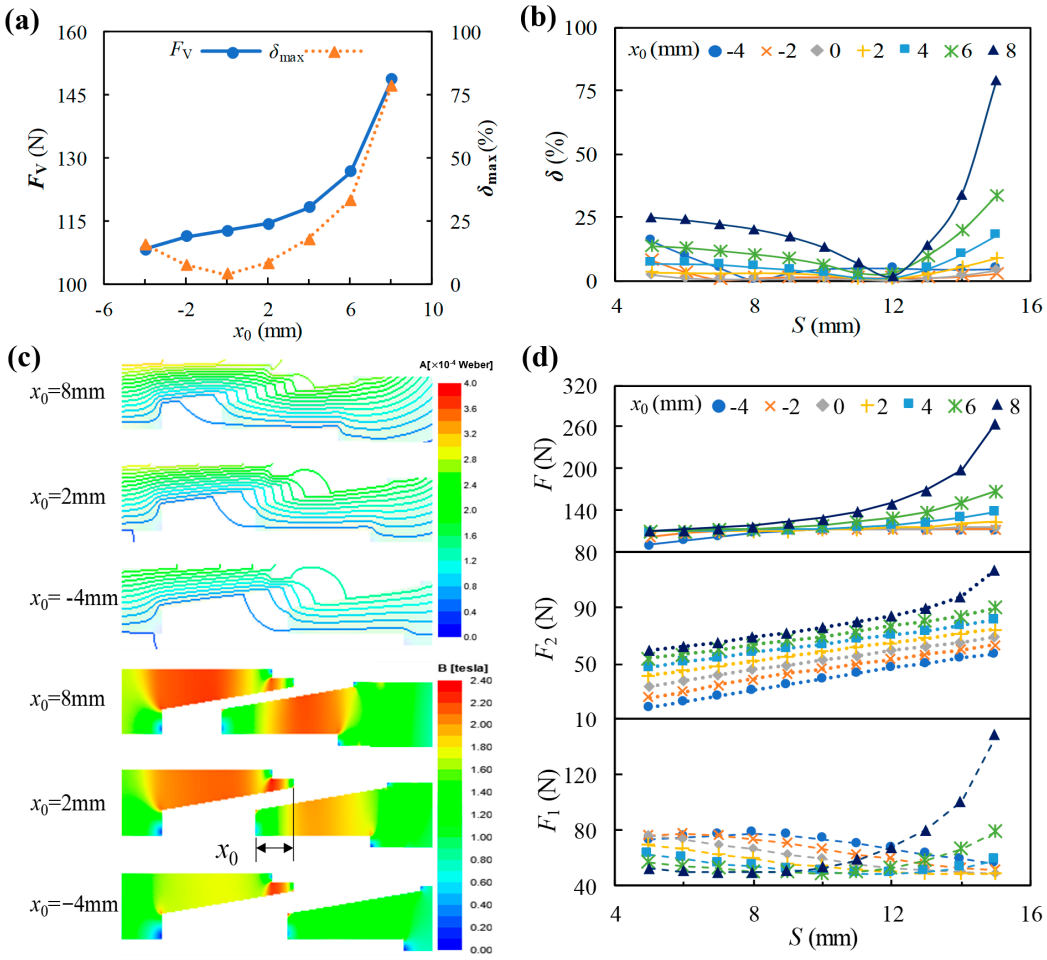


Figure 12. The influence of initial position of the armature on the constant force characteristics: (**a**) the average-output solenoid force and maximum-output solenoid force variability; (**b**) output solenoid force variability; (**c**) the magnetic field cloud map; (**d**) and the electromagnetic component forces.

Furthermore, it is seen from Figure 12d that additional axial solenoid force F_2 approximately increases linearly with the increase in the stroke. The growth rate remains unchanged when the initial position of the armature has less than a certain value. However, for small initial position values of the armature, the axial solenoid force F_1 gradually decreases as the stroke increases, and the rate of decline gradually intensifies. On the other hand, for large initial position values of the armature, the axial solenoid force F_1 initially decreases with an increase in the stroke; however, when the working stroke is substantial, there is a significant reduction in the working air gap between the forward direction of the armature and the bottom of the coil skeleton. Consequently, this leads to an increase in magnetic flux Φ_{12}, including the axial solenoid force F_1.

Consequently, with an increase in the initial position value of the armature, the increase in the additional axial solenoid force F_2 first approaches the decrease rate of the axial solenoid force F_1, and then the output solenoid force increases. Hence, maximum-output solenoid force variability first decreases, and then increases.

5.2. Correlation Analysis

5.2.1. Main Factors

Figure 13 shows the variation in the correlation coefficient between the main factor and the average-output solenoid force, maximum-output solenoid force variability, and two evaluation indexes. Firstly, it is seen from Figure 10 that there is a relatively strong positive correlation between the average-output solenoid force and maximum-output solenoid force variability, and the correlation coefficient between them is 0.55, indicating that increasing or decreasing the average-output solenoid force will simultaneously lead to increases or decreases in maximum-output solenoid force variability. Therefore, there is a strong contradictory relationship between the two evaluation indexes. This is because the correlation directions between the main factors, the average-output solenoid force, and maximum-output solenoid force variability are the same. The cone length is negatively correlated with the average-output solenoid force and maximum-output solenoid force variability, while the other main factors are correlated positively with the average-output solenoid force and maximum-output solenoid force variability. The change in the main factors will lead to the phenomenon of the average-output solenoid force and maximum-output solenoid force variability increasing or decreasing simultaneously. This makes the average-output solenoid force and maximum-output solenoid force variability develop a strong coupling relationship. Therefore, these two evaluation indexes need to be synthetically considered in optimization design.

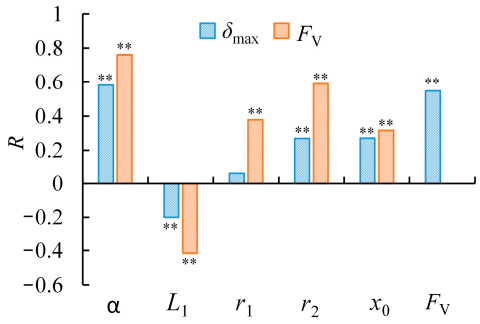


Figure 13. The correlation coefficients of the main factors and the evaluation indexes. ** denotes a statistically significant correlation at the levels of 0.01 based on a two-tailed significance test.

Secondly, it is seen from Figure 13 that the cone angle has the strongest correlation with the average-output solenoid force and maximum-output solenoid force variability, with correlation coefficients of 0.76 and 0.58, respectively. This means that a change in the cone angle affects the average-output solenoid force and maximum-output solenoid force variability. Therefore, more attention should be paid to the cone angle in optimization design. The correlation between the other main factors and the average-output solenoid

force is relatively strong. The correlation coefficients of the average-output solenoid force and the outer cone diameter, the cone length, the cone inner diameter, and the armature's initial position are 0.59, −0.42, 0.38, and 0.32, respectively. Changes in these factors will also significantly affect the average-output solenoid force. However, the correlation strength between the other main factors and maximum-output solenoid force variability is relatively weak, particularly the correlation strength between the inner diameter of the cone and maximum-output solenoid force variability, which is the weakest, is 0.06. The correlation coefficients of the other main factors, between the initial position of the moving core, the outer cone diameter, the cone length, and maximum-output solenoid force variability are 0.27, 0.27, and −0.2, respectively. The changes in these factors have relatively little influence on maximum-output solenoid force variability. Because the correlation strength between the cone inner diameter and the average-output solenoid force is strong, but the correlation strength between the cone inner diameter and maximum-output solenoid force variability is relatively weak, increasing the inner cone diameter can increase the average-output solenoid force without significantly increasing maximum-output solenoid force variability, and will not cause a strong contradiction between the average-output solenoid force and maximum-output solenoid force variability. Therefore, it is important to pay attention to this when optimizing the design.

5.2.2. Interaction Factors

Figure 14 shows the change in correlation coefficient between each interaction factor and the average-output solenoid force, as well as maximum-output solenoid force variability. It can be seen from Figure 13 that the interaction factors α*L_1, α*r_1, α*r_2, L_1*r_2, and r_1*r_2 have strong correlations with the average-output solenoid force, with correlation coefficients of −0.44, 0.53, 0.36, −0.48, and 0.42, respectively. Simultaneously, the correlation coefficients between α*r_2, L_1*r_2, and maximum-output solenoid force variability are also stronger, with correlation coefficients of 0.37 and −0.4, respectively. This indicates that for these interaction factors, when one parameter is at a different level, the influence of the other parameter on the constant force characteristics significantly changes. The correlation coefficients between the remaining interaction factors and the average-output solenoid force and maximum-output solenoid force variability are weak, and the correlation coefficients are less than 0.3, particularly the correlation coefficients between the interaction factor r_2*x_0, the average-output solenoid force, and maximum-output solenoid force variability, which are close to 0. It is seen that the interaction between the cone angle and the cone length, the cone angle and the cone inner diameter, the cone angle and the cone outer diameter, the cone length and the cone outer diameter, and the cone inner diameter and the cone outer diameter have an important influence on the constant force characteristics of long-stroke MPSAs. Hence, revealing the interaction mechanism of these interaction factors on the constant force characteristics is the premise to determine the specific improvement direction of each parameter.

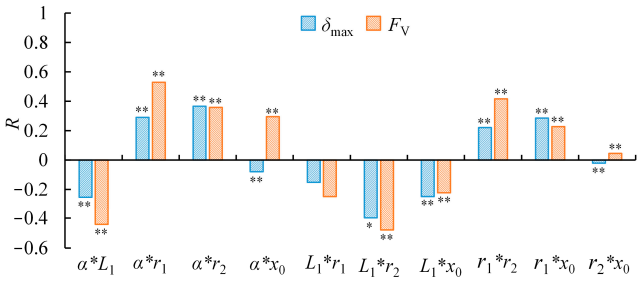


Figure 14. The correlation coefficients of the interaction factors. * and ** denote statistically significant correlations at the levels of 0.05 and 0.01 based on a two-tailed significance test, respectively.

6. Conclusions

This paper focuses on a long-stroke MPSA. The two evaluation indexes, the average-output solenoid force and maximum-output solenoid force variability, were introduced to reveal the influence rules of the key design parameters on the constant force characteristics of the long-stroke MPSA. The influence of parameters and parameter interaction factors on the constant force characteristics was quantified. The conclusions drawn from the results can be summarized as follows:

(1) The average-output solenoid force gradually increases with the increase in the cone angle, the inner cone diameter, the outer cone diameter, and the initial position of armature, but decreases with the increase in the cone length. Maximum-output solenoid force variability first decreases, and then increases gradually with the increase in the cone angle, the outer cone diameter, and the initial position value of the armature; moreover, it decreases gradually with the increase in the cone length and increases with the increase in the inner cone diameter.

(2) There is a strong contradiction between the average-output solenoid force and maximum-output solenoid force variability, with a correlation coefficient of 0.55; however, increasing the inner diameter of the cone helps enhance the average-output solenoid force without significantly increasing maximum-output solenoid force variability.

(3) The cone angle is the most significant parameter affecting the constant force characteristics, and its correlation coefficients with the average-output solenoid force and maximum-output solenoid force variability are 0.76 and 0.58, respectively. Simultaneously, the interaction between the cone angle and the cone length, the cone angle and the inner cone diameter, the cone angle and the outer cone diameter, the cone length and the outer cone diameter, as well as the inner cone diameter and the outer cone diameter also have an important influence on the constant force characteristics.

Author Contributions: Conceptualization, P.L., R.S. and W.Q.; methodology, P.L., R.S. and W.Q.; validation, P.L. and Y.O.; investigation, W.Q. and Y.O.; resources, P.L. and R.S.; data curation, P.L. and Y.O.; writing—original draft preparation, W.Q. and Y.O.; writing—review and editing, P.L. and R.S.; visualization, W.Q.; funding acquisition, P.L and R.S. All authors have read and agreed to the published version of the manuscript.

Funding: This work was supported by the Foundation of Liaoning Provincial Key Laboratory of Energy Storage and Utilization (grant number CNNK202421), the Excellent Youth Project of the Education Department of Hunan Province of China (grant number 23B0305), and the Natural Science Foundation of Hunan Province of China (grant number 2021JJ40588).

Data Availability Statement: The data are included within this article.

Conflicts of Interest: The authors declare no conflicts of interest.

References

1. Cococi, V.; Călinoiu, C.; Safta, C. Electro-pneumatic servomechanism with proportional direction control valve. In Proceedings of the 2023 13th International Symposium on Advanced Topics in Electrical Engineering (ATEE), Bucharest, Romania, 23–25 March 2023; pp. 1–6.
2. Lee, G. Design improvement of a linear control solenoid valve using multiphysics simulation. *Mechanics* **2018**, *24*, 352–359. [CrossRef]
3. Bayat, F.; Tehrani, A.F.; Danesh, M. Finite element analysis of proportional solenoid characteristics in hydraulic valves. *Int. J. Automot. Technol.* **2012**, *13*, 809–816. [CrossRef]
4. Chen, G.; Zhang, W.; Yu, B. Multibody dynamics modeling of electromagnetic direct-drive vehicle robot driver. *Int. J. Adv. Robot. Syst.* **2017**, *14*. [CrossRef]
5. Yun, S.; Ryu, J.S.; Ahn, B.K.; Kim, G.D.; Jo, J.H. Electrohydraulic proportional metering valve for common rail system. *Proc. JFPS Int. Symp. Fluid Power* **2005**, *2005*, 269–274. [CrossRef]
6. Chen, C.; Chiang, M. Development of proportional pressure control valve for hydraulic braking actuator of automobile ABS. *Appl. Sci.* **2018**, *8*, 639. [CrossRef]
7. Meng, F.; Tao, G.; Luo, P.P. Dynamic analysis of proportional solenoid for automatic transmission applications. In Proceedings of the 2014 International Conference on Mechatronics and Control (ICMC), Jinzhou, China, 3–5 July 2014; pp. 1120–1124.

8. Lankin, M.V.; Lozin, O.I.; Lankina, M.Y. Magnetization dynamic characteristics models for hydraulic drives of proportional electromagnets. *Procedia Eng.* **2017**, *206*, 443–448. [CrossRef]
9. Park, C.; Lim, B.; Chung, K. Design verification methodology for a solenoid valve for industrial applications. *J. Mech. Sci. Technol.* **2015**, *29*, 677–686. [CrossRef]
10. Lee, J.; Yun, Y.; Hong, H.; Park, M. Control of spool position of on/off solenoid operated hydraulic valve by sliding-mode controller. *J. Mech. Sci. Technol.* **2015**, *29*, 5395–5408. [CrossRef]
11. Lee, G.S.; Sung, H.J.; Kim, H.C. Multiphysics analysis of a linear control solenoid valve. *J. Fluids Eng.* **2013**, *135*, 011104. [CrossRef]
12. Arakawa, T.; Niimi, S. Optimization technology of magnetic circuit for linear solenoid. In Proceedings of the SAE 2002 World Congress, Detroit, MI, USA, 4–7 March 2002; pp. 1–7.
13. Xu, J.; Kou, F.; Zhang, X.; Wang, G. Modeling and testing for continuously adjustable damping shock absorber equipped with proportional solenoid valve. *J. Mech. Sci. Technol.* **2023**, *37*, 3851–3866. [CrossRef]
14. Wang, S.; Weng, Z.; Jin, B. A performance improvement strategy for solenoid electromagnetic actuator in servo proportional valve. *Appl. Sci.* **2020**, *10*, 4352. [CrossRef]
15. Zhang, H.; Manuel, P.; Pineda-Sanchez, M. The characteristic improvement of electromagnetic proportional directional control valve. *J. Control Sci. Eng.* **2018**, *2018*, 3582454. [CrossRef]
16. Yuan, X.; Ling, H.; Qiu, T.; Zhou, J.; Zhao, R. Optimization for a proportional electro-magnet with high accuracy utilizing finite element method. *Int. J. Appl. Electromagn. Mech.* **2021**, *65*, 267–280. [CrossRef]
17. Yun, S.; Ham, Y.; Park, J. New approach to design control cone for Electro-Magnetic proportional solenoid actuator. In Proceedings of the IEEE/ASME International Conference on Advanced Intelligent Mechatronics, Taiwan, China, 11–14 July 2012; pp. 2159–6255.
18. Yun, S.; Ham, Y.; Park, J. Attraction force improvement strategy of a proportional solenoid actuator for hydraulic pressure control valve. In Proceedings of the 2012 12th International Conference on Control, Automation and Systems, Jeju Island, Republic of Korea, 17–21 October 2012; pp. 1123–1127.
19. Yu, Y.X.; Ke, S.D.; Jin, K.D. Structural parameters optimization for a proportional solenoid. *Int. J. Simul. Model.* **2020**, *19*, 689–700. [CrossRef]
20. Meng, B.; Heng, Y.; Li, S. Novel modulation approach of flat force–displacement characteristic of linear electro-mechanical converter for electro-hydraulic servo-proportional valve. *Proc. Inst. Mech. Eng. Part I J. Syst. Control. Eng.* **2022**, *236*, 1922–1939. [CrossRef]
21. Ding, C.; Ding, F.; Zhou, X.; Liu, S.; Yang, C. Novel pressure-resistant oil-immersed proportional actuator for electrohydraulic proportional control valve. *J. Mech. Des.* **2013**, *135*, 125001. [CrossRef]
22. Wang, S.; Weng, Z.; Jin, B. Multi-objective optimization of linear proportional solenoid actuator. *Appl. Comput. Electrom.* **2020**, *35*, 1338–1339.
23. Wang, S.J.; Weng, Z.D.; Jin, B.; Cai, H.X. Multi-objective genetic algorithm optimization of linear proportional solenoid actuator. *J. Braz. Soc. Mech. Sci. Eng.* **2021**, *43*, 60. [CrossRef]
24. Liu, P.; Ouyang, Y.; Quan, W. Multi-objective optimization of a long-stroke moving-iron proportional solenoid actuator. *Micromachines* **2024**, *15*, 58. [CrossRef]
25. Song, E.; Zhao, G.; Yao, C.; Ma, Z.; Ding, S.; Ma, X.; Ruben, S.; Specogna, R. Study of nonlinear characteristics and model based control for proportional electromagnet. *Math. Probl. Eng.* **2018**, *2018*, 2549456. [CrossRef]
26. Peng, Y.; Wang, Y.; Hu, F.; He, M.; Mao, Z.; Huang, X.; Ding, J. Predictive modeling of flexible EHD pumps using kolmogorov-arnold networks. *arXiv* **2024**, arXiv:2405.07488v2. [CrossRef]
27. Lan, Q.; Fan, L.; Bai, Y.; Gu, Y.; Wen, L. Correlation analysis upon the influential factors related to the dynamic response characteristics of pressure amplification piston in the fuel system for a low-speed diesel engine. *Fuel* **2020**, *276*, 118052. [CrossRef]
28. McKay, M.D.; Conover, W.J.; Beckman, R.J. Latin Hypercube Sampling: A comparison of three methods for selecting values of input variables in the analysis of output from a computer code. *Technometrics* **1979**, *21*, 239–245.
29. Liu, P.; Ouyang, Y.; Deng, J. Demarcation method for magnetostatic model of long-stroke moving-iron proportional electromagnetic actuator. *IEEE Trans. Ind. Electron.* **2023**, *70*, 7122–7130. [CrossRef]

Disclaimer/Publisher's Note: The statements, opinions and data contained in all publications are solely those of the individual author(s) and contributor(s) and not of MDPI and/or the editor(s). MDPI and/or the editor(s) disclaim responsibility for any injury to people or property resulting from any ideas, methods, instructions or products referred to in the content.